

# Identifying the third dimension in 2D fluoroscopy to create 3D cardiac maps

Jasbir Sra,<sup>1,2</sup> David Krum,<sup>1,2</sup> Indrajit Choudhuri,<sup>1,2</sup> Barry Belanger,<sup>2</sup> Mark Palma,<sup>2</sup> Donald Brodnick,<sup>2</sup> and Daniel B. Rowe<sup>2</sup>

<sup>1</sup>Aurora Cardiovascular Services, Aurora Sinai/Aurora St. Luke's Medical Centers, <sup>2</sup>APN Health, LLC, Milwaukee, Wisconsin, USA.

Three-dimensional cardiac mapping is important for optimal visualization of the heart during cardiac ablation for the treatment of certain arrhythmias. However, many hospitals and clinics worldwide cannot afford the high cost of the current mapping systems. We set out to determine if, using predefined algorithms, comparable 3D cardiac maps could be created by a new device that relies on data generated from single-plane fluoroscopy and patient recording and monitoring systems, without the need for costly equipment, infrastructure changes, or specialized catheters. The study included phantom and animal experiments to compare the prototype test device, Navik 3D, with the existing CARTO 3 System. The primary endpoint directly compared: (a) the 3D distance between the Navik 3D-simulated ablation location and the back-projected ground truth location of the pacing and mapping catheter electrode, and (b) the same distance for CARTO. The study's primary objective was considered met if the 95% confidence lower limit was greater than 0.75% for the Navik 3D-CARTO difference between the 2 distances, or less than or equal to 2 mm. Study results showed that the Navik 3D performance was equivalent to the CARTO system, and that accurate 3D cardiac maps can be created using data from equipment that already exists in all electrophysiology labs.

## Introduction

Heart rhythm disorders, including atrial fibrillation (AF), are rapidly increasing in incidence as the population ages. Catheter ablation using 3D mapping is an effective treatment for certain cardiac arrhythmias and often involves targeting specific anatomic structures (1–7). There are several 3D cardiac mapping systems currently in use, among them the CARTO 3 System V3.0 (Biosense Webster, Inc.) and EnSite NavX (St. Jude Medical, Inc.) (4–5). These technologies, while effective, can be cost prohibitive and have limited applicability in many hospitals throughout the world (8). Biplane fluoroscopy provides another method for improved cardiac visualization, but the equipment is expensive and increases radiation exposure to the patient, and is thus not commonly available in electrophysiology (EP) labs. Furthermore, it does not provide 3D mapping.

Alone, single-plane fluoroscopy, which is available in all EP labs, does not provide the 3D visualization essential for mapping and ablation of cardiac arrhythmias. For example, in a typical fluoroscopy image taken during a procedure, it is only possible to view the catheter location along the *x-y* plane; the *z* axis is not discernible. We hypothesized that real-time images from 2-dimensional (2D) fluoroscopy combined with data from electrocardiograms and signals from intracardiac electrograms (EGMs) could be used to create comparable 3D maps of the cardiac chamber.

The research team developed a prototype of the 2D-3D cardiac mapping device called Navik 3D. The end result is a multicomponent computer system (Figure 1) that incorporates custom image-processing techniques and mathematical algorithms to reconstruct the 3D location and spatial orientation of cardiac catheters. Through digitization and synchronization of patient data from existing fluoroscopy and ECG-EGM systems, Navik 3D generates real-time maps that enable physicians to identify the location of the mapping and ablation catheter as it is placed and moved inside the heart (Figure 2). This potentially novel approach relies upon the use of diagnostic equipment that already exists in all EP labs and does not require special catheters or patches.

The system's hardware comprises off-the-shelf computers, monitors, and data acquisition tools and devices. Navik 3D uses image- and signal-processing methods that utilize existing EP lab data to generate 3D maps for the diagnosis and mapping of cardiac arrhythmias. The system uses real-time single-plane fluoroscopic

**Conflict of interest:** J. Sra has significant ownership in APN Health, which partially funded the study. D. Krum and I. Choudhuri are consultants of APN Health. B. Belanger, M. Palma, D. Brodnick, and D. Rowe are contract employees of APN Health.

**Submitted:** September 1, 2016

**Accepted:** November 8, 2016

**Published:** December 22, 2016

### Reference information:

JCI Insight. 2016;1(21):e90453.  
doi:10.1172/jci.insight.90453.



**Figure 1. Navik 3D in the context of the electrophysiology lab.** Navik 3D utilizes data from existing fluoroscopy and electrocardiogram-electrogram equipment to generate 3D cardiac maps for use during electrophysiology procedures. The system provides 2 user interfaces (U/I) to the interventional team: (i) Main application U/I (upper left) generated by the system's Main computer workstation, which displays real-time fluoroscopy images and the 3D cardiac map, and (ii) a U/I on the Apple iPad (upper right), which serves as controller only and enables physician-directed operation from any location in the electrophysiology lab. AP, anteroposterior; CL, cycle length; LAT, local activation time.

images and ECG-EGM signals from the existing patient recording and monitoring system. The device's image and signal processing algorithms identify the  $x$ ,  $y$ ,  $z$  location of the catheter tip and provide the cycle length (CL), local activation times (LATs), and EGM voltage that form the basis for "3D Catheter Location Determination" and 3D cardiac mapping. The technique of using existing data from the laboratory, avoiding any special catheters and patches, and using off-the-shelf hardware (such as computers) allows the system to be built in a cost-effective way.

In addition to design verification and validation testing throughout Navik 3D prototype development, the team conducted an extensive phantom and animal study to test the primary hypothesis. In this study, the navigation and mapping capabilities of Navik 3D and a commercially available control device, CARTO, were directly compared. Raw data were collected and analyzed to report the mapping and simulated ablation accuracies of the prototype in a phantom and in a beating heart and are being presented in the manuscript.

## Results

*Phantom study.* The phantom study compared the prototype system, Navik 3D, to the CARTO 3 System, using a CARTO catheter (NAVISTAR THERMOCOOL, Biosense Webster, Inc.) in a full range of positions and 6 angles in a phantom test fixture. At each point, independent ground truth 3D position was

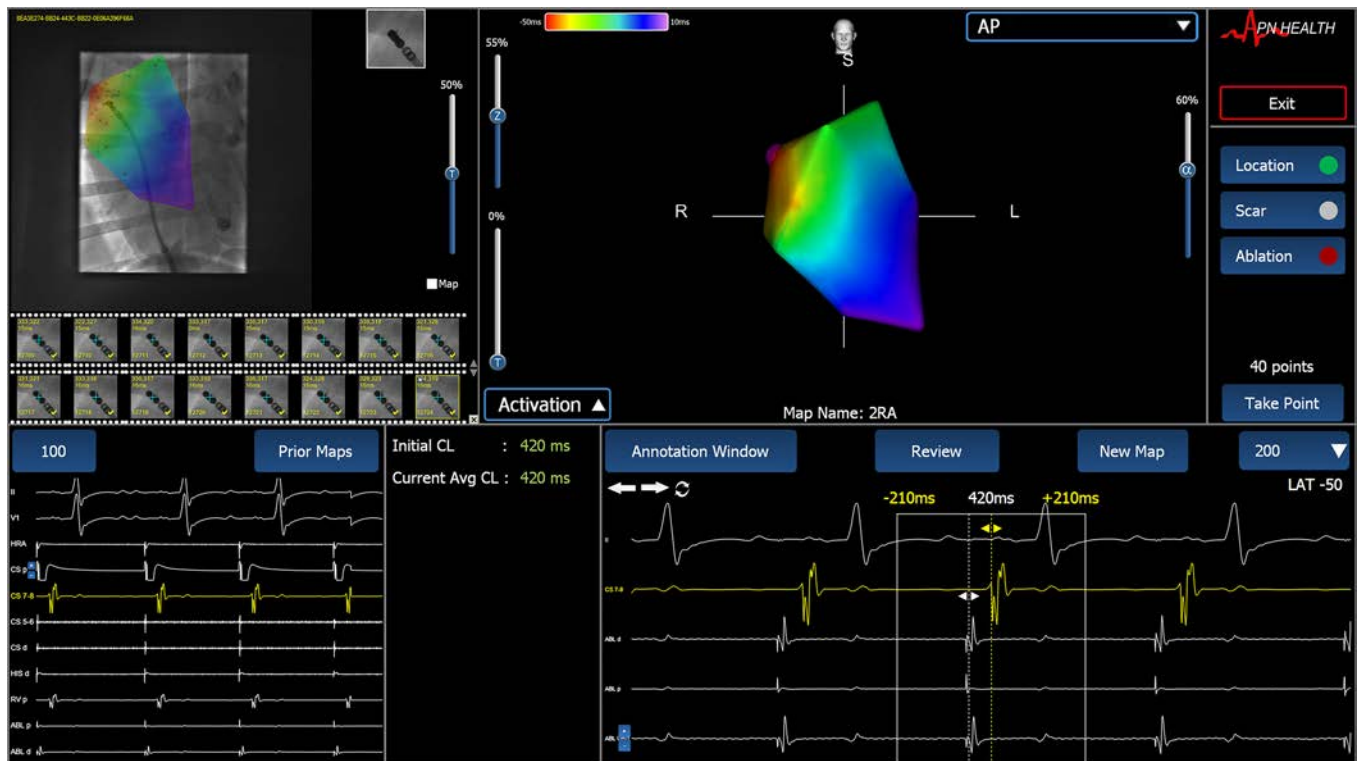


**Figure 2. Screenshot of Navik 3D user interface and a right atrial map created during the experiments.** The 3D map (top, center) also can be projected in 2D on the fluoroscopy screen (top left). Red indicates the earliest or lowest value region of the map, blue the last or highest value. The colors in the 3D maps above represent: purple = late activation time, blue/green/yellow = intermediate activation time, and red = early activation time. AP, anteroposterior; CL, cycle length; LAT, local activation time.

obtained via back projection from oblique 2D view pairs to allow effective comparison of Navik 3D and CARTO 3D positions.

Two simultaneous 3D maps were created using the NAVISTAR THERMOCOOL catheter (Figure 3). The study characterized the key features of Navik 3D's three-dimensional location performance, and showed that displacement compensation for the difference in mean positional error between Navik 3D and CARTO was less than 1 mm (0.3 mm) (Table 1).

Similarly, during repeatability testing between Navik 3D and CARTO, the differences also were minimal, less than 1 mm between Navik 3D versus CARTO using the NAVISTAR THERMOCOOL catheter (0.281 mm vs. 0.333 mm). Position accuracy was further tested using 2 additional, commonly used, non-CARTO catheters, St. Jude Medical's Safire BLU SP Bi-directional 7 French Ablation Catheter and Biosense Webster's CELSIUS, with minimal differences between Navik 3D and CARTO: 0.267 mm and 0.174 mm, respectively. The mean distance from the ground truth was not statistically different for the 3 catheter tips (0.16 mm range between the 3 catheters).

**Animal study.** In the animal study, the CARTO catheter was used to create simultaneous activation maps (2 in the right atrium [RA] and 2 in the left ventricle [LV] in 8 animal models) during pacing using implanted plunge electrodes. The endpoint data evaluated clinically relevant target values using the earliest points on the map to which the catheter was navigated in a randomized fashion using either Navik 3D or CARTO. The earliest locations as determined by both devices were then tagged to create simulated ablations.

In the study, 31 of 32 maps were successfully completed: 16 in the RA and 15 in the LV. One animal went into ventricular fibrillation during pacing and could not be resuscitated. The mean and SD fluoroscopy time per map was  $7.1 \pm 4.4$  minutes. The mean number of points taken for creation of maps was  $20 \pm 5$  for RA and  $21 \pm 5$  for LV. The mean pacing CL during RA1 and RA2 maps was  $474 \pm 77$  ms and  $352 \pm 36$  ms. The mean procedure time for individual maps was  $34.6 \pm 20.0$  minutes. The mean time for RA maps was  $29.1 \pm 15.9$  minutes and for LV maps was  $40.2 \pm 22.4$  minutes. Table 2 depicts a summary of procedure time, fluoroscopy time, map points, and pacing CL for each chamber mapped.

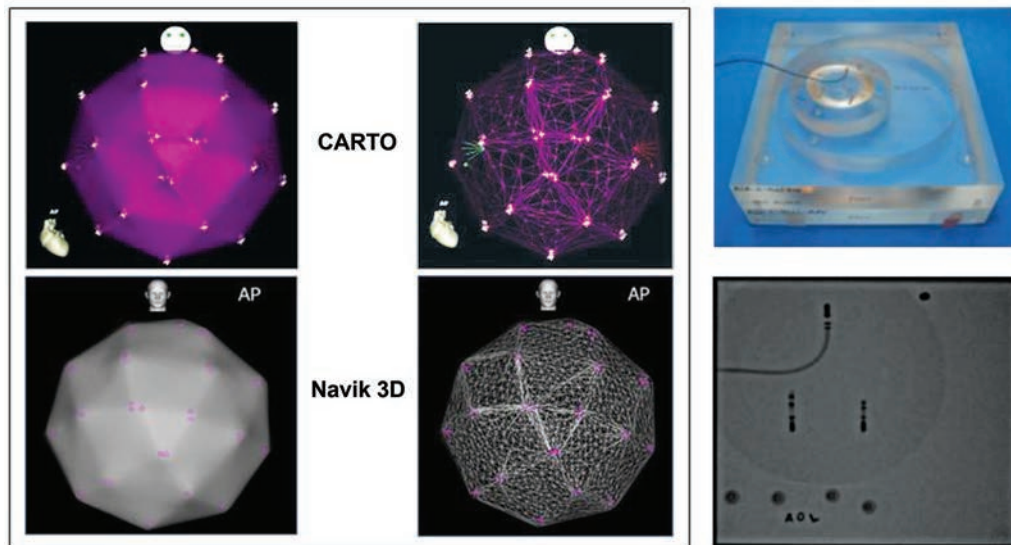


**Figure 3. Simultaneous 3D maps and phantom test fixture.** Left panel: CARTO map (top) and Navik 3D map (bottom) using 36 points taken simultaneously. Right panel: Phantom test fixture used in the study (top). Fluoroscopic image of the 3 catheters and the phantom (bottom), with a live CARTO catheter at the top of the image.

Each animal entered into a single, nonsurvival surgery during which the following 2 procedures, mapping and simulated ablation, were performed and study data were collected.

The key measured items from these procedures were: (a) the distance (DN) between the Navik 3D simulated ablation location and the back-projected location of the pacing and mapping electrode (ground truth), and (b) the same distance (DC) for the CARTO device.

#### The Navik 3D-CARTO difference (DN-DC) between the 2 distances

There were 93 simulated ablation points taken by each device, Navik 3D and CARTO, as the process was repeated 3 times per map after hiding the previous point tagged (31 maps with 3 simulated ablation points per map). Each simulated ablation point from one modality was paired with each simulated lesion from the other modality at a given target site, resulting in 279 possible paired data values. All nine ( $3 \times 3$ ) possible DN-DC differences per map were included in the analysis to obtain the most unbiased estimate. For the primary analysis, 246 out of 279 values had DN-DC distances of less than or equal to 2 mm. These results are summarized as proportions along with their 1-sided 95% bootstrap lower CI below (9).

#### Primary Hypothesis

Because the observed primary hypothesis proportion 0.88 was larger than its 1-sided 95% bootstrap lower CI bound of 0.83, the  $\pi \leq 0.75$  null hypothesis was rejected and it was concluded the prototype was equivalent to (not statistically different from) the CARTO system.

**Table 1. 3D tip location analysis distance results (in mm), using 36 mapping locations with 3 replicates at each location (108 points).**

	Distance	n	Mean	Bootstrap 95% CIs for Mean		SD	Median	Minimum	Maximum
Navik 3D	DN <sup>A</sup>	108	2.236	2.010	2.468	1.245	2.023	0.156	5.911
	x	108	0.755	0.623	0.892	0.737	0.473	0.003	2.978
	y	108	0.687	0.600	0.775	0.467	0.671	0.008	1.774
	z	108	1.783	1.558	2.024	1.255	1.549	0.025	5.383
	DC	108	1.939	1.730	2.155	1.154	1.488	0.380	5.578
CARTO	x	108	0.507	0.406	0.619	0.579	0.319	0.002	2.805
	y	108	0.473	0.380	0.577	0.540	0.277	0.004	2.764
	z	108	1.709	1.519	1.899	1.032	1.397	0.020	3.951
	DN - DC	108	0.300	0.012	0.573	1.492	0.514	-3.237	2.840

<sup>A</sup>DN, Navik 3D distance between pacing electrode and mapping electrode; DC, CARTO 3D distance between pacing electrode and mapping electrode.



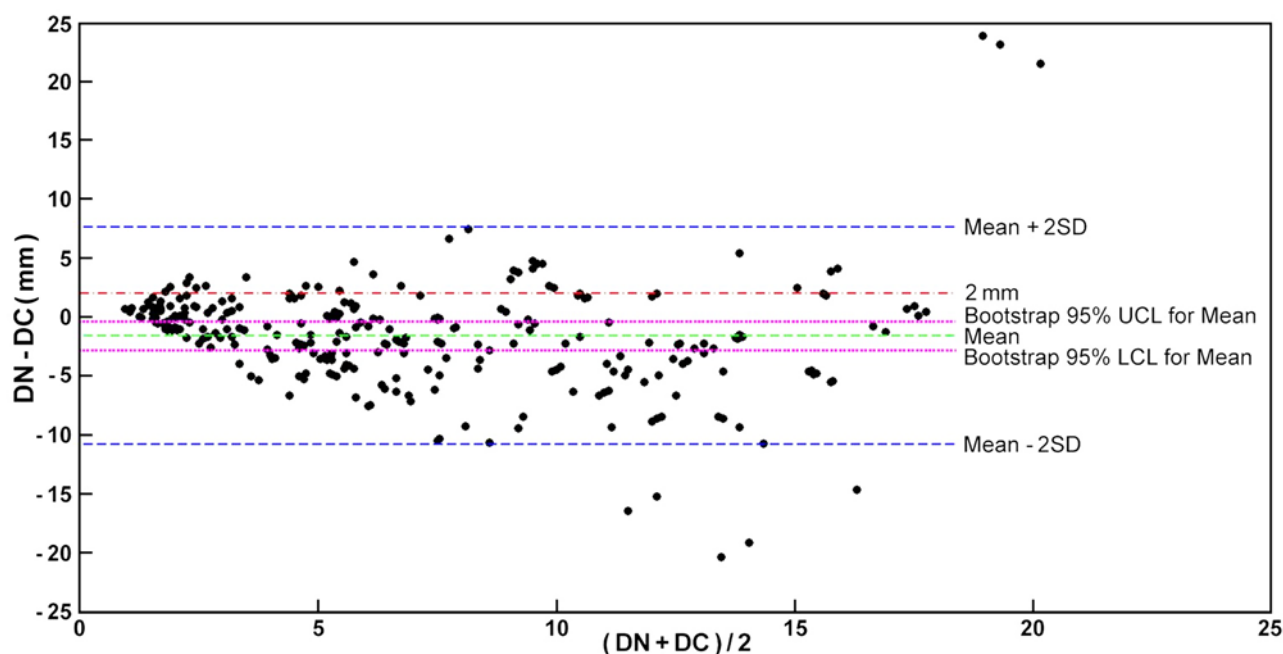


**Figure 4. Secondary analysis: Bland-Altman plot.** The 279 DN –DC differences were plotted against the average  $(DN + DC)/2$  in a scatter plot. The mean line, its 2-sided bootstrapped 95% upper and lower CI limits (UCL and LCL, respectively), mean  $\pm$  2 SD lines, and +2 mm lines are depicted on the graph. DN, Navik 3D distance between pacing electrode and mapping electrode; DC, CARTO 3D distance between pacing electrode and mapping electrode.

An additional secondary analysis was performed in which the DN-DC differences were plotted against the average  $(DN + DC)/2$  in a Bland-Altman plot (10). The mean line, its bootstrapped 2-sided 95% CI lines, mean  $\pm$  2 SD lines, and +2 mm lines are depicted in the graph in Figure 4.

From the Bland-Altman plot (Figure 4), it can be seen that the mean difference ( $y$  axis) is negative, indicating a generally smaller distance for Navik 3D than CARTO. From the Bland-Altman plot, we also can see a small indication that the lesser the distance of the  $x$  axis, the lesser the difference of the  $y$  axis between Navik 3D and CARTO.

A generalized estimating equation (GEE) regression analysis (DN vs. DC) was performed with an animal as a subject using the SAS GENMOD (SAS v9.2) procedure and presented in Figure 5 in order to view the relationship, if any, between Navik 3D and CARTO distances. The regression analysis yielded the line in red with a slope of 0.56 (95% 2-sided CI 0.30 to 0.83,  $P$  value = 0.01) and an intercept of 1.88 (95% 2-sided CI of 0.44 to 3.32,  $P$  value < 0.0001). In Figure 5, we can see a general pattern that when there are larger (or smaller) CARTO distances, there are larger (or smaller) Navik 3D distances. We also can see that the points generally fall below a 45-degree (zero intercept and slope of 1) line in blue indicating a trend that Navik 3D generally reports a smaller distance than CARTO. It can be seen that the 2-sided 95% CI for the slope does not contain zero, indicating that there is a positive relationship between CARTO and Navik 3D distances. Furthermore, we can see that the 2-sided 95% CI for the intercept does not contain 1, indicating that the Navik 3D and CARTO performance is not the same.

**Table 2. Summary of procedure time, fluoroscopy time, map points, and pacing cycle length for each chamber**

Study Chamber <sup>A</sup>	RA 1	RA2	LV1	LV2
Procedure time (minutes)	31.6 $\pm$ 13.2	26.5 $\pm$ 18.7	50.4 $\pm$ 26.0	30.0 $\pm$ 12.4
Fluoroscopy time (minutes)	5.51 $\pm$ 2.60	6.48 $\pm$ 6.09	9.32 $\pm$ 3.47	7.32 $\pm$ 3.39
Number of map points	21.8 $\pm$ 5.2	18.7 $\pm$ 4.7	22.9 $\pm$ 5.1	20.6 $\pm$ 5.3
Pacing CL (ms)	474.4 $\pm$ 77.3	352 $\pm$ 36.0	435.6 $\pm$ 56.8	423.3 $\pm$ 55.9

<sup>A</sup>RA, right atrium; LV, left ventricle; CL, cycle length.

Bland-Altman graphical summaries and quantitative regression analyses thus showed that the Navik 3D prototype was capable of performing in a beating heart with performance equivalent to the control.

## Discussion

The study demonstrated the feasibility of 3D mapping using single-plane fluoroscopy. The study also demonstrated that the prototype device, Navik 3D, is capable of performing in a beating heart with performance equivalent to the control device, the CARTO system.

AF, the most commonly occurring cardiac arrhythmia worldwide, is nearing epidemic proportions. By 2050, this heart rhythm disorder is anticipated to affect up to 20 million individuals in the United States alone (1, 3). AF is associated with risks, including heart failure, stroke, and death, and imposes significant healthcare costs worldwide.

When control by medication is not effective, the treatment with the greatest potential to decrease the AF burden is catheter ablation. In patients with cardiac arrhythmias, including AF, for optimal visualization of the heart during ablation, use of 3D cardiac mapping is essential. Several 3D mapping systems currently are available on the market. However, the combination of high upfront costs (\$500,000 to \$800,000) and the added expense of specialty catheters and/or patches required for operation makes these systems unaffordable to many, if not most, medical facilities. In addition, the complex nature of the existing systems often requires hiring a dedicated operator to run the equipment and EP lab infrastructure modifications upon installation.

It is estimated that less than 10% of patients with cardiac arrhythmias undergo 3D mapping (8). Many institutions and countries have started to put limits on how much money can be spent on an individual ablation procedure. Navik 3D offers an affordable yet equally effective alternative, as evidenced by the research presented in this study. One of the development team's primary goals was to design a system that would be easy to use and compatible with the currently available EP lab equipment, thus making it accessible to greater numbers of hospitals. Cost containment was a top priority. The resulting technology relies upon use of existing fluoroscopy and patient recording and monitoring data, does not require specially designed catheters or patches, and is operated on standard, off-the-shelf hardware.

Navik 3D technology utilizes existing EP lab data to generate 3D maps for the diagnosis and mapping of cardiac arrhythmias. Navik 3D's main hardware components include a commercially available all-in-one Windows-based personal computer, an off-the-shelf frame grabber for capturing analog images, and an ECG card for signal processing. An Apple iPad can be used as a controller for convenient operation in the EP lab. An optional monitor, keyboard, and mouse may be added if desired. The current cost to build the entire Navik 3D system is less than \$15,000.

The Navik 3D system is intended to be used as an additional resource to the EP lab's existing fluoroscopy and patient recording and monitoring equipment. The live images and signals from these systems remain available for the operator throughout the procedure and do not experience interference from the Navik 3D operations. Installation of Navik 3D in the EP lab is a simple 1-time setup that typically does not require infrastructure modification.

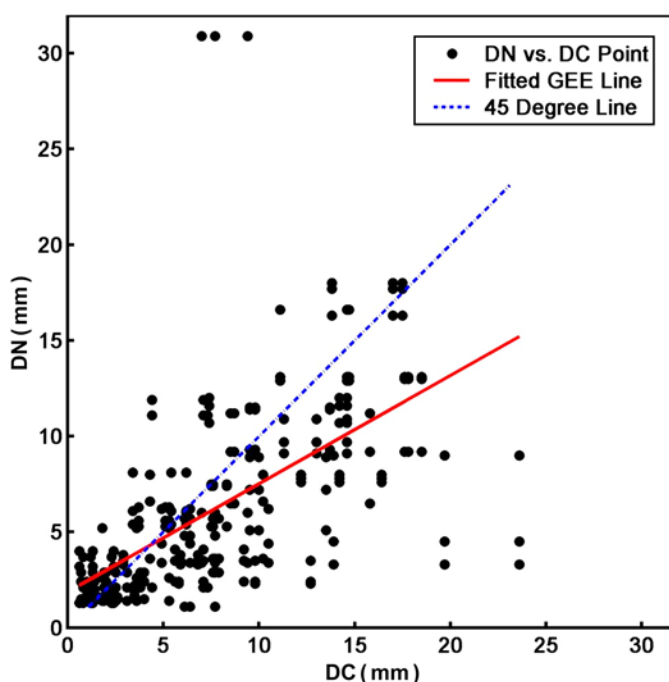


**Figure 5. Secondary analysis regression plot for DN vs. DC (in mm).**

Scatter plot of 279 DN – DC differences, where DN is the Navik 3D distance between pacing electrode and mapping electrode and DC is the CARTO 3D distance between pacing electrode and mapping electrode. A generalized estimating equation (GEE) regression analysis yielded the line in red with a slope of 0.56 (95% 2-sided CI 0.30 to 0.83,  $P$  value = 0.01) and an intercept of 1.88 (95% 2-sided CI of 0.44 to 3.32,  $P$  value < 0.0001).

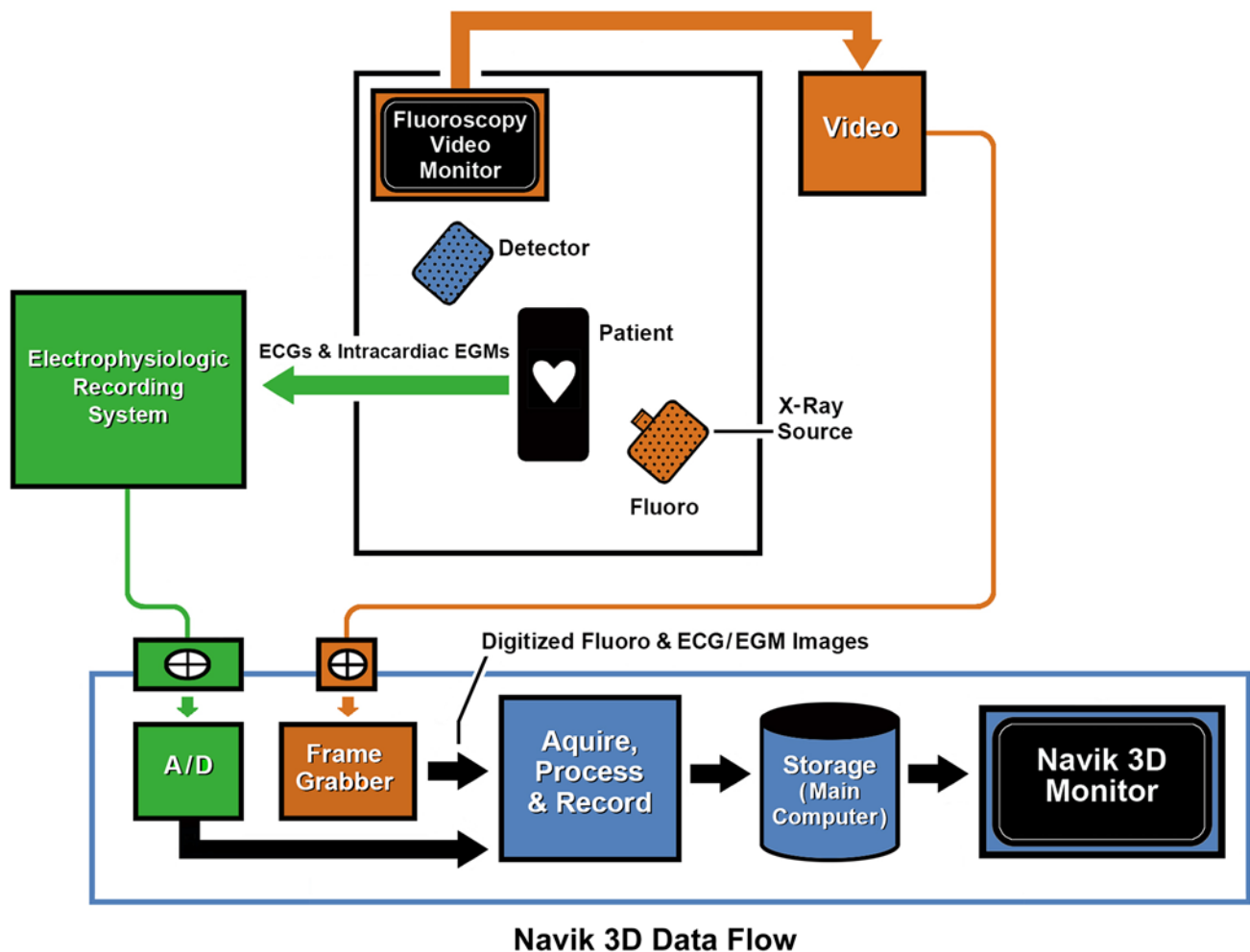


**Figure 6. Navik 3D data flow diagram.** Real-time patient data are acquired, processed, recorded, and stored by the Navik 3D device. Orange reflects the flow of fluoroscopy image data, and green reflects the flow of signal data. The fluoroscopy and electrocardiogram-electrogram (ECG-EGM) data are synchronized and time stamped. The frame grabber for fluoroscopy data and analog-to-digital converter for ECG-EGM data are housed in the Main computer. A/D, analog to digital.

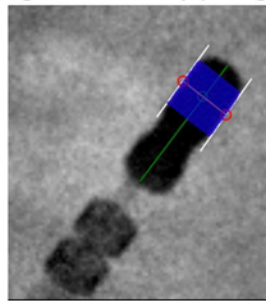
Fluoroscopy is commonly used during cardiac ablation to provide visualization of the heart's anatomy, and some manufacturers of 3D mapping devices suggest that fluoroscopy time can be reduced in certain circumstances. It is important to note that testing of Navik 3D shows the system does not require fluoroscopy exposure beyond the standard of care to generate detailed 3D maps. In fact, the mean fluoroscopy time in our studies was comparable to or less than the existing fluoroscopy times reported for similar studies (11). Navik 3D is likely to reduce fluoroscopy time (and dose) from standard amounts owing to the following: the catheter is visible in 3D and 2D when using Navik 3D; therefore, the physician is provided with better orientation information and is likely to use less fluoro.

As Navik 3D continuously records fluoro, it requires about a second or less of fluoroscopy to detect 3D location. Fluoroscopy data can then be analyzed offline, unlike the current practice for existing systems. Thus, no fluoroscopy images are wasted, and multiple points can be taken and corrected offline as needed without requiring additional fluoroscopy. Further studies will be needed in patients to corroborate these observations.

The impact of increased access to this technology along with other associated advances within the field offers the best opportunity to make a material impact the world over on the burden and associated expense of AF and other arrhythmia treatment, with the ultimate goal of improving clinical outcomes. Furthermore, this technology also may be applicable to other types of interventions, such as the placement of a pacing lead, angioplasty balloon, or stent, both in the heart and the periphery.

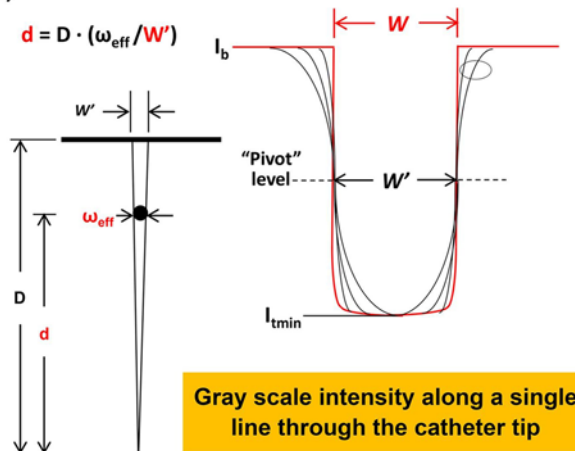
In summary, the potentially novel system described in this manuscript provides a simple, affordable technology that will enable all EP labs to implement important 3D mapping for mapping and

Image of Catheter Tip (enlarged)



Averaged Catheter Tip Profile

Width measured at multiple cross sections



**Figure 7. Accurate catheter width and depth measurement.** Taking multiple cross sections perpendicular to the center line (left image) greatly improves the accuracy of the effective width ( $\omega_{\text{eff}}$ ) measurement of a catheter tip. This information is then used to identify the depth of the catheter tip by the equation depicted here.  $D$ , source to detector distance;  $d$ , source to object distance;  $W$ , true projected width;  $W'$ , width that can be reliably measured.

ablation procedures. As demonstrated by the phantom and animal study, Navik 3D is capable of performing in a beating heart with performance equivalent to the CARTO system. As healthcare organizations face immense challenges to reduce costs coupled with the rapidly rising demand for ablation treatment of arrhythmias such as AF, there is keen interest in finding alternative techniques that will broaden 3D mapping accessibility. Navik 3D offers the innovation of utilizing ample and readily available 2D data to generate 3D maps. The system determines the 3D placement of a catheter using only 2D information obtained from a fluoroscope, which is present in all interventional labs. Navik 3D works with most commercially available catheters and any fluoroscopy system. Additionally, the concept is simple, allowing operation of the system with minimal or no support outside of the traditional lab staff needed for the procedure and minimal if any infrastructure modification. Looking forward, the techniques described here could also potentially be used in non-EP procedures.

## Methods

### Objective

The study was designed to investigate the performance of the 2D-3D prototype (Navik 3D) in a phantom and in a beating heart and to demonstrate that its performance is equivalent to the control device (CARTO). The goal of the data processing described herein was to demonstrate the relative accuracy of the mapping catheter's 3D location under the guidance of Navik 3D compared with CARTO.

### Navik 3D technology

**Device overview.** Navik 3D comprises several subsystems. The Application Subsystem runs the majority of the device's software applications, serving as the primary user interface (U/I) for all patient data, the 3D cardiac maps, and other information technology tools necessary for overall system operation. The central component of the Application Subsystem is the Main Application Computer/Workstation (Main computer), an all-in-one Windows-based personal computer that includes a monitor. An optional monitor with similar displays and operated with a wireless or wired keyboard and mouse can be added if needed.

The Data Acquisition (DAQ) Subsystem plays a key role in the Navik 3D mapping process. It acquires and digitizes the EP lab's existing fluoroscopy and patient recording and monitoring system data, which is essential to determining the 2D and 3D catheter locations. This subsystem comprises a small DAQ computer customized with off-the-shelf hardware and peripheral devices, including a frame grabber and National Instruments ECG card, plus software components to enable acquisition and digitization of streaming fluoroscopy and ECG/EGM data. It also time stamps the data packets and transfers the digitized data to the Main computer. Figure 6 illustrates how real-time data travel from the EP lab's systems to the DAQ Subsystem for digitizing, processing, recording, and storage, then on to the Main computer for relevant data display.

The Navik 3D Tablet Device Subsystem utilizes an iPad to provide a secondary U/I that allows the user to control the system from any location in the EP lab. The iPad is customized with software to enable user interaction with the main application. The tablet acts as a command console or graphical mouse for the system. It is, however, designed for ease of use and is not essential for functioning of the system.



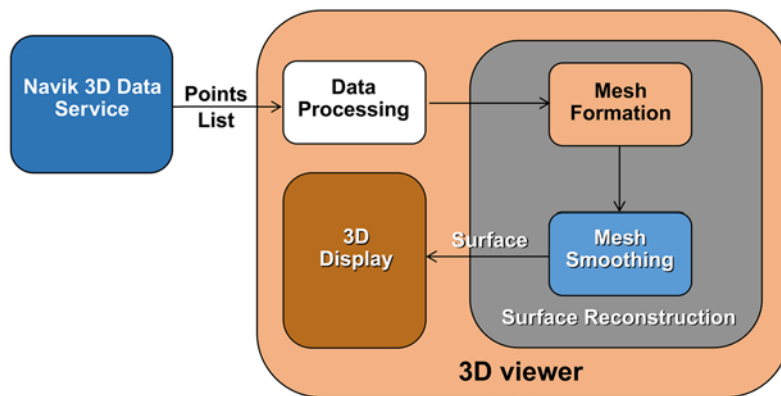


**Figure 8. 3D mapping surface reconstruction process.** This diagram illustrates the steps for reconstruction of the 3D surface using points acquired during mapping in Navik 3D. The surface generated is customizable to different resolutions based on distances between mapped points.

### 3D Catheter Location Determination

The foundational idea behind the system's 3D Catheter Location Determination is the recognition that the 2D projection of the single-plane fluoroscopy system contains information about the position of the object in 3D. X-ray conic projection and physics principles are used in the software algorithms to generate the 3D location of the catheter from these 2D images. The 3D

position of the catheter tip is determined based on the detected (magnified) size of the catheter tip in the fluoroscopic image, the known distance from the x-ray source to the fluoroscopy detector, and the known width of the catheter tip.

X-rays travel from a small, quasi-point x-ray source in a cone beam toward the patient, where they interact with the tissues of the patient and any objects within. EP catheter electrodes are made with materials such as platinum and iridium, which present a very high attenuation to the x-ray beam. As a result, essentially no x-rays pass through the electrodes. The catheter electrodes are high-contrast objects, owing to their high radiopacity. This is by design; it is best if the electrodes are unambiguously visible in the fluoroscopic image.

Due to the conic projection from the x-ray source to the image detector, an object, such as a catheter-tip electrode, will appear larger if closer to the x-ray source and smaller if closer to the detector. If the true size of the catheter tip is known, as well as the distance from the x-ray source to the detector, the distance of the catheter tip from the x-ray source can be calculated.

Owing to the relatively small diameter of a catheter-tip electrode (2.33 mm to 3.00 mm), the typical x-ray source-to-detector distance (100 cm) and the typical positioning of the patient relative to the x-ray detector, the divergence of the cone beam around the catheter tip is relatively small. Because of this, the calculation of the depth of the catheter tip from its apparent width in the image is very sensitive. For a 7-F (2.33 mm) diameter catheter and typical imaging geometry, achieving a depth accuracy of approximately 4 mm requires a width measurement accuracy of approximately 0.02 mm. Considering that the typical fluoroscopy detector for EP procedures has a detector element or pixel spacing of 0.182 mm to 0.200 mm, it is clear that width measurement accuracy must be sub-pixel. Although this situation is challenging, there are several mitigating factors.

The size of a typical electrode segment is such that multiple width measurements can be made and averaged to improve the width estimate. For example, electrode segments are typically at least 4 mm long. Allowing for geometric magnification, this creates an image at the detector at least 5 mm long, provided the axis of the electrode is parallel to the detector. In general, the

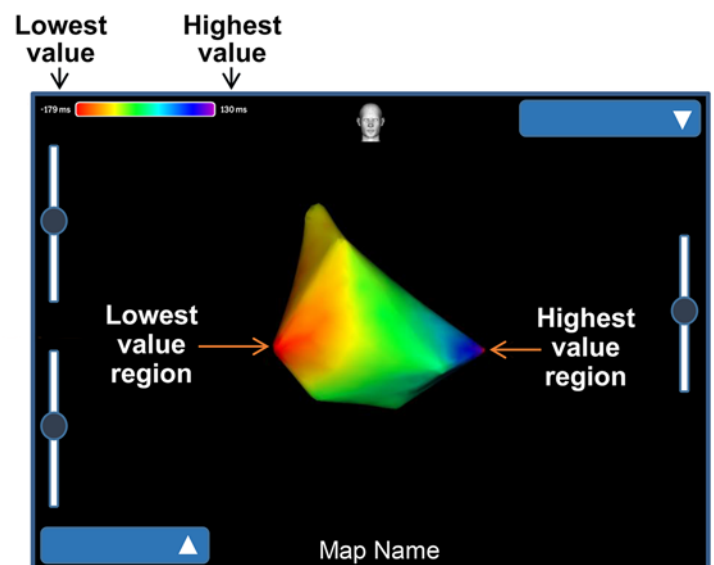


**Figure 9. Reconstruction and depiction of color-coded maps.** The scale shows the lowest (earliest LAT) and highest (latest LAT) values, which have been color-coded for ease of view. LAT, local activation time.

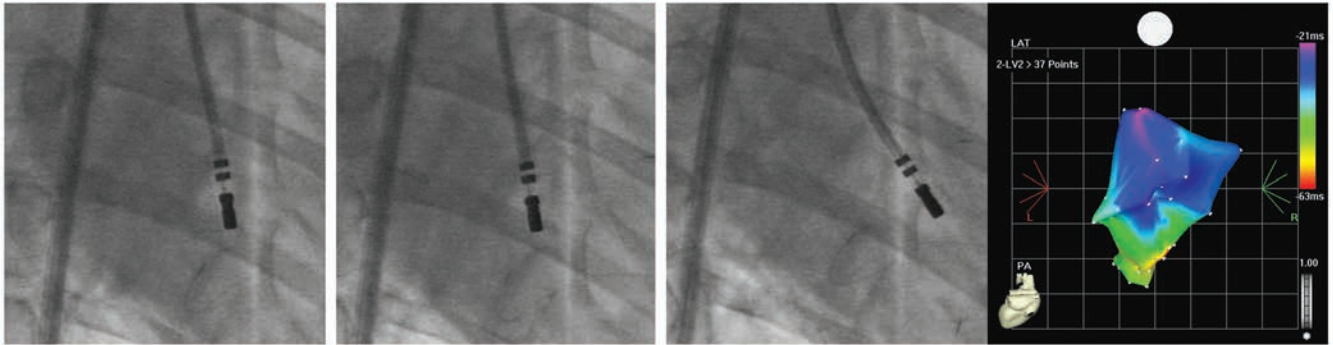


**Figure 10. Outlier points during simulated ablation.** The locations of the mapping catheter at 3 outlier points are shown above, taken during the simulated ablations guided by CARTO for experiment 3, left ventricle Map 2.

axis of the electrode will not be parallel to the detector, so a reasonable typical electrode length in the image is 4 mm. Assuming 0.2-mm detector element spacing, this provides a minimum of 20 individual width measurements that can be averaged (Figure 7).

If  $W$  is the true projected size of the electrode width and if the catheter tip is moving at 20 mm/second and the fluoroscopy x-ray exposure time is 10 ms, the electrode will move 0.2 mm during an exposure, or 8% of its width, causing some blurring.

A solution to this problem is illustrated in the profiles on the right of Figure 7. Note that there is an intensity level in the profiles at which a stable width  $W'$  (width that can be reliably measured) can be measured. This intensity level is called the pivot level.

Considering the above, the following techniques are used to optimize accuracy of depth estimation from width measurements. First, the relationship between  $W$  and  $W'$  is established through a process called initialization, in which 2 oblique fluoroscopy views of the catheter electrode are taken at the beginning of a procedure. The width of the electrode is measured in the primary view, while the secondary view is used to independently determine the depth of the catheter electrode through the back-projection process. Having the independently determined depth and  $W'$ , effective width value, or  $\omega_{\text{eff}}$  can be calculated. Effective width is the value of the width of an electrode at the known depth determined in initialization that would yield the  $W'$  value that was actually measured. Thus,  $\omega_{\text{eff}}$  takes into account the x-ray effects that occur at the edges of the electrode. It also will account for any discrepancy between the quoted size of the detector pixel and its actual size. In addition, because it does not require the manufacturer's quoted dimension of the catheter electrode, it will compensate for any manufacturing process variations that may occur over the period of production of a given catheter type.

To deal with the fact that all fluoroscopy systems have nonlinear intensity remapping functions, it is possible to empirically determine the pivot level at system installation by performing experiments in which the blurring is deliberately varied while a catheter electrode is kept at a fixed depth. The pivot level is then identified as the level at which the least width variability is seen.

Once the  $\omega_{\text{eff}}$  of the catheter tip is determined, the system can generate 3D maps by identifying the location of the mapping catheter. When the Take Point button is activated on the Navik 3D mapping system and the  $x$ ,  $y$ ,  $z$  location is determined by the 2D-3D algorithm, the 3D point is added to the 3D reconstruction algorithm. This creates the 3D object and renders a smooth surface.

Mapping points can be selected based upon examination of the activation times and CL obtained from the ECG-EGM waveforms. Using these mapping points, the physician can view the basic location maps and different renderings. Additional information, including tip location, activation times, and voltage, also can be displayed as was done in these experiments.

### Waveform analysis

During a procedure, the physician selects mapping points based upon examination of the LAT and CL obtained from the ECG-EGM waveforms. An example of this is shown in the Annotation Window (lower right) in Figure 2. A stable electrical reference is chosen, and, based on the CL of the tachycardia, an Annotation Window is set up. The reference is usually placed in the middle of the window, but its location could

be changed. LAT, the distance between the electrical waveforms generated by the mapping catheter and the reference catheter, is calculated as the mapping catheter is navigated around the chamber. As the catheter gets closer to the source, the LAT should become negative. As the mapping catheter moves away from the source, the LAT becomes positive. Signal-processing algorithms are built into Navik 3D coordinate and communicate activities via interprocess messages that are transported by a set of shared message queues. A data cache holds raw input data (fluoroscopic images and patient ECG-EGMs), which are time synchronized.

### 3D map creation

The user interface of the Main computer provides information and menus that enable operation of the Navik 3D software functions for 3D map creation and depiction. The U/I screen displays the real-time fluoroscopy and ECG-EGM data (Figure 2), allowing the physician to take points. After analyzing the 3D location of the catheter and Annotation Window depicting waveforms, the physician then determines which points to use in the creation of the maps. The physician also determines the orientation of the 3D map and the map style (e.g., activation, voltage, 3D, or mesh), and has access to tools for zooming in and out of the image and adjusting transparency. The resulting cardiac maps allow the physician to navigate to the point of interest (repeatedly if needed) and mark areas of interest, such as the placement of an ablation lesion, a particular anatomic structure, or an electrical signal of interest at a particular location. The device also creates a display that shows the correlation of the 3D anatomic location with the electrical activation of the heart.

Figure 8 depicts the steps of reconstruction of the 3D surface from points acquired during mapping in Navik 3D. The surface generated is customizable to different resolutions based on distances between mapped points.

Electrical information of the map, based on properties such as activation and voltage recorded at taken points, is depicted using a color palette (Figure 9). Based on point properties, color mapping of scalar values on the reconstructed surface is used to create 2 types of maps: activation and voltage.

A color lookup table is created with the color palette in correspondence to the scalar values that are being mapped. The range of values is the difference between the highest and lowest value recorded for the map. The size and color of the earliest or lowest value region in the map are configurable for visual demarcation. The color lookup table is applied to the surface mapper to get the data visualized with colors. The highest and lowest value mapped and the color palette used are portrayed by a color bar. Additionally, the system allows conic projection of the 3D representation of a cardiac chamber that is being mapped under the fluoroscope. The projection is generated to match the current fluoroscopy view on Navik 3D. The 2D projection image is used as an overlay on the fluoroscopy view in Navik 3D.

### Phantom study

The phantom portion of the study was conducted using an anthropomorphically designed phantom test fixture, which was positioned in an x-ray system with 3 mounted catheters to characterize the Navik 3D performance for catheter tip 3D location. During the study, Navik 3D was compared with the CARTO system control (predicate) device using a CARTO catheter (NAVISTAR THERMOCOOL). Testing was performed in a full range of 36 positions and angles and repeated 3 times using a phantom test fixture positioned in an x-ray system (Figure 3). At each point, independent ground truth 3D position data, which were obtained via back projection from oblique 2D view pairs, were collected to allow effective comparison of Navik 3D and CARTO 3D positions. The 3D position accuracy of Navik 3D was also tested with the 2 other non-CARTO catheters, Safire BLU SP Bi-directional 7 French Ablation Catheter, and CELSIUS.

The primary endpoint was the Euclidian distance between the 3D positions given by Navik 3D and CARTO from the gold standard, which is a 2-view back-projection position. The secondary endpoints were: (a) the Euclidian distances between the Navik 3D locations and their respective back-projection locations using each of the 3 catheters, i.e., NAVISTAR THERMOCOOL, Safire BLU SP Bi-directional 7 French Ablation Catheter, and CELSIUS, and (b) reproducibility of the Navik 3D and CARTO locations in triplicate measures. For each of the 3 catheters, the distance between each Navik 3D location and the corresponding back-projection ground truth was calculated and summarized with 2-sided 95% CIs for the means. In addition, Bland-Altman plots were used to illustrate the difference in Navik 3D's and CARTO's distance to the ground truth.

### Animal study

For the animal portion of the study, 8 mongrel canines with a body weight of 20 to 30 kg entered into the study in good health condition. The animal study was conducted at Aurora Health Care's Animal Research Facility and was approved by the facility's IACUC prior to the receipt of animals and study initiation. All surgical procedures were carried out using techniques that were approved and recommended by the facility's veterinarian for nonsurvival surgeries. For the duration of the study, the IACUC and veterinarian oversaw the welfare of animals associated with the experiments. At the conclusion of the study, all animal health reports (e.g., vendor receipts, animal receipt forms, and physical examination records) were compiled, and the overall health of the animals was summarized by the site veterinarian. The final animal health report was signed and dated by the veterinarian.

### Surgical technique

General anesthesia was administered by a trained nurse anesthetist using intramuscular injections of acepromazine (2 mg/kg) and followed 15–20 minutes later by intravenous administration of propofol. The surgical plane of anesthesia was maintained with isoflurane (2%–3% and 6–8 liters per minute of oxygen). For the duration of the surgery, pulse oximetry and arterial blood pressure were monitored, and body surface ECGs and intracardiac EGMs were monitored continuously using a CardioLab EP recording system (GE Healthcare).

After sternotomy, the sinus node was crushed in each experimental animal if the heart rate exceeded 120 beats per minute or was variable and fast. For the mapping experiments, the heart was paced at a fixed rate.

The heart was suspended in a pericardial cradle. Plunge electrodes (used for pacing) and unipolar pacing leads (used for subsequent pacing site location identification using back projection — the method used for accurate 3D localization of the pacing and mapping electrodes using 2 sequential fluoroscopy views) were implanted. Three plunge electrode/pacing lead pairs were installed in each chamber. However, following a randomization process, only 2 of these 3 pairs were used for mapping. After the electrodes were placed, the chest cavity was closed.

A separate set of plunge electrodes was implanted in the left atrium and in the right ventricle. The EGMs from these electrodes were used as a reference for RA and LV maps.

### Mapping and simulated ablation procedures

*Randomization for chamber mapped.* A simple, equal-probability randomization scheme was used to randomly assign the series of chambers (RA, LV) for each mapping and ablation experiment. Based on the randomization, mapping and simulated ablation were performed in one chamber before moving to the next.

*Model preparation.* After introducer sheaths were placed into the femoral vein and artery, right internal jugular vein, and the left carotid artery, they were filled with saline containing 1,000 units of heparin to reduce the chance of clotting during the experiment. Activated clotting time (ACT) was checked and heparin was administered intravenously at 1.5 mg/kg or as needed to achieve an effective anticoagulation protection with ACT of 300 to 400 seconds (12).

An 8.5 F Zurpaz deflectable sheath (Boston Scientific Corp.), was inserted into the RA or LV, depending upon which randomly assigned chamber was being mapped first for the given experiment.

### Mapping

*Randomization for pacing electrodes.* Two of the 3 electrode positions were randomly selected for pacing and map creation. The location of electrodes and source of the pacing (i.e., the randomly assigned electrode) were known only to the animal surgeon who implanted the electrodes; the physician operator creating the map with Navik 3D and the technicians operating the Navik 3D and CARTO systems were blinded to the source. Randomization was prepared prior to study initiation, and the appropriate randomization information was submitted and viewed at the beginning of the procedure by the study coordinator and shared with the animal surgeon. The fluoroscopic image and sketch of the electrodes used for mapping were included in the study's data forms for subsequent evaluation.

Following the surgical preparation and the placement of the pacing electrodes and randomization process described above, the animal surgeon did not participate in the subsequent steps of the Navik 3D and CARTO mapping and simulated ablation portion of the procedure.

*Mapping.* The ability of Navik 3D to acquire activation maps of a cardiac chamber during paced cardiac rhythm was examined by constructing both RA and LV activation maps during RA or LV cardiac pacing,



respectively. Pacing was performed at twice the diastolic threshold. Four activation map sets per animal (2 maps per chamber) were simultaneously generated using the same points with both the prototype and control systems. This was possible due to use of the NAVISTAR THERMOCOOL catheter, which could be used simultaneously for both Navik 3D and CARTO mapping.

The mapping catheter was advanced into the chamber of interest (i.e., RA or LV). Then, the Navik 3D initialization was performed. The initialization step involved imaging the catheter tip in 2 oblique views, so that its 3D position could be determined by back projection. Then, using this 3D position, the effective width ( $\omega_{\text{eff}}$ ) of the catheter tip was calculated. In this case,  $\omega_{\text{eff}}$  is the catheter tip width that, at the measured 3D position, would produce the width measured in the projected image in the anteroposterior (AP) view. The use of  $\omega_{\text{eff}}$  accounts for any manufacturing variation in the actual catheter tip width and any effects of x-ray penetration of the edge of the catheter tip.

The initialization process involved taking about 5 seconds of fluoroscopy data in left anterior oblique (LAO) 20 degrees and AP projection in a sequential fashion. For all 8 studies, analysis of the CARTO-simulated ablation point location was performed in exactly the same fashion (i.e., using back-projected catheter and pacing electrode locations during each simulated lesion) as was done for Navik 3D.

During pacing from transmyocardially placed pacing electrodes, 2 maps were created for each chamber and endocardial points obtained for each map until the physician operating the system was satisfied with the maps (Figure 3, left panel). Of the 2 maps created in the RA, 1 was at a pacing rate of at least 30–50 ms faster than the sinus or junctional escape rate, and the other at a (typically faster) CL of approximately 300 ms. In case of a significant drop in blood pressure or variability in the heart rate, the pacing rate was adjusted as needed. To avoid hemodynamic instability, ventricular maps were only created at pacing CLs 30–50 ms shorter than the sinus or junctional escape interval. At every point, the stability of the EGM was verified before capturing the map point. Furthermore, each point was captured during the animal's end expiration and with ECG gating.

This mapping procedure was repeated in both chambers, and the total fluoroscopy exposure time was recorded for each activation map in the study's data files.

*Control of bias.* To control bias, the physician operator was blinded to the specific electrode used for pacing during both mapping and simulated ablation procedures (i.e., pacing occurred from 1 of the 3 electrodes for each map). During the mapping portion of the study, only a single fluoroscopy view was used and back projection was not utilized to verify catheter location.

## Simulated ablation

*Randomization.* For the simulated ablation procedure, the order in which the Navik 3D and CARTO maps were used to navigate and tag the ablation locations was randomized prior to study initiation.

*Simulated ablation.* A simulated ablation procedure permitted assessment of navigation of Navik 3D and CARTO to areas of earliest activation as defined by the respective maps.

Once an activation map was created in each chamber of the study animal, the physician removed the catheter from the cardiac chamber. The physician then reinserted the catheter and, using the first randomly assigned map (Navik 3D or CARTO) that was just created, navigated the catheter (in the AP fluoroscopy view only) to the location that he believed was the site of earliest activation. He tagged that location as a simulated ablation point (i.e., no lesion was administered). Following this, without moving the catheter, images were captured in 2 views, AP and LAO 20 degrees, so the back-projection technique could be used later to provide the ground truth 3D locations of the catheter tip at the simulated ablation location. The back-projection  $x$ ,  $y$ , and  $z$  coordinates of the pacing and distal electrodes of the mapping catheter were used in the subsequent analysis.

The catheter again was removed and the ablation point that had just been tagged on the map was hidden from the physician's view. After the point was hidden, the physician reinserted the catheter and repeated the process of tagging the ablation site. This part of the procedure was repeated 3 times for each system's map. Following simulated ablation with the first system's map, the identical series of events was carried out using the other system's map (Navik 3D or CARTO). This process was repeated in both chambers for every map in each animal.

In addition to marking pacing electrode locations on the sketch before mapping and simulated ablation, after all simulated ablation locations were documented, the animal surgeon examined the magnified AP/LAO image pairs of electrodes on fluoroscopy at the end and marked the location of the pacing leads on a saved fluoroscopy view (a feature available on Navik 3D).

Following the creation of all maps and identification of all simulated ablation locations, the animal was euthanized, while anesthetized, via induction of ventricular fibrillation.

### Statistics

The ground truth location was calculated and used to determine the distance accuracy between Navik 3D versus ground truth, and CARTO versus ground truth. The primary and secondary endpoints were as follows. Primary endpoints: the distance between the simulated Navik 3D ablation location and the back-projected location of the pacing electrode (ground truth), the same distance for the CARTO device, and the Navik 3D-CARTO difference between the 2 distances. Secondary endpoints: The  $x$ ,  $y$ , and  $z$  coordinates of the primary endpoints.

*Primary hypothesis.* The study's primary hypothesis was that real-time images from 2D fluoroscopy combined with data from ECGs and signals from intracardiac EGMs could be used to create 3D maps of the cardiac chamber that are comparable to those generated by the 3D mapping devices currently in use in EP labs. In the testing of the primary hypothesis, the following were analyzed: (a) let DN denote the distance between the simulated Navik 3D ablation location and the back-projected location of the pacing electrode (ground truth); (b) let DC denote the same distance for the CARTO device; and (c) let  $\pi$  be the true proportion of data points, where  $DN - DC \leq 2$  mm.

The 1-sided hypotheses for the primary analysis were as follows:  $H_0: \pi \leq 0.75$ ;  $H_a: \pi > 0.75$ . In order to reject the null hypothesis  $H_0$  at a 0.05 statistical significance level, the observed proportion in the study for  $DN - DC \leq 2$  mm needed to be higher than 0.80 (13).

*Primary analysis.* For testing the  $H_0$ , the proportion of data pairs (DN, DC) with  $DN - DC \leq 2$  mm was calculated using all available data. At each targeted ablation location, since both DN and DC were measured in triplicate and the testing was not paired, all 9 ( $3 \times 3$ ) possible DN-DC differences were included in the analysis to obtain the most unbiased estimate. A 1-sided 95% confidence lower limit was calculated by the bootstrap method with the animal as the resampling unit (8). The study's primary objective was considered met if 1-sided 95% confidence lower limit was greater than 0.75. In order to meet this objective, the actual proportion observed in the study generally needed to be higher than 0.80 (13).

*Secondary analysis.* Descriptively, the DN and DC measurements and their differences (DN-DC) were summarized as mean, SD, median, minimum, and maximum. The proportions for DN less than or equal to 2 mm and DC less than or equal to 2 mm were also reported.

Graphically, Bland-Altman analysis (10) was performed. The DN-DC differences were plotted against the average  $[(DN + DC)/2]$  in a scatter plot. The mean line, its 2-sided bootstrapped 95% CI lines, mean  $\pm 2$  SD lines, and  $\pm 2$  mm lines are depicted on the graph (Figure 4).

In addition, a regression analysis (DN regressed on DC) was performed using a generalized estimating equation model with an animal as a subject using the SAS GENMOD (SAS v9.2) procedure. The resulting 2-sided 95% CIs are reported for the intercept and the slope. The regression analysis yielded the line in red with a slope of 0.56 (95% 2-sided CI 0.30 to 0.83,  $P$  value = 0.01) and an intercept of 1.88 (95% 2-sided CI of 0.44 to 3.32,  $P$  value < 0.0001). Regression results are also graphically displayed (Figure 5) with the red line in addition to a zero-intercept unity slope 45-degree reference line in blue.

*Data analysis approach.* For this analysis, calculation of the minimal distance between the pacing and mapping electrode difference between Navik 3D and CARTO as compared with back projection using the closest approach (minimal distance) was performed. This was determined to be an appropriate approach since in experimental and clinical scenarios, the lesions would extend circumferentially from the ablation tip electrode (14).

The plunge electrodes used for pacing were not placed on the endocardium and the endocardial breakthrough was a distance away from the pacing electrode (15). Targeting the endocardial breakthrough, as was done in this study, provided an unbiased way of comparing the 2 devices, as the endocardial breakthrough site would be similar for both maps.

### Study methods: data collection, transfer, processing, and analysis

This section summarizes the methods used to process image data acquired from the set of 8 clinical experiments explained above.

## Experimental data collection

Once the point was marked in the AP view, it could not be changed. For the subsequent catheter tip and pacing electrode ground truth determination using the back-projection technique, the fluoroscopy images were obtained in the LAO view. This acquisition did not change in any way the simulated ablation point, which already was taken in the AP view at the best location determined by using the map created with the system. Before the next sequence for simulated ablation was done, the previous point was hidden for both Navik 3D and CARTO and the catheter moved from the site. The sequence was then repeated in a similar fashion 3 times for each device.

Fluoroscopy sequences acquired during the experiments were tagged with time of acquisition, and each frame was associated with a unique identification number. Experimental procedure records, maintained by the study personnel present during each study, contain time-stamped logs of all identified simulated ablation points and the fluoroscopy data associated with them.

There were 3 simulated ablation points per map per device (Navik 3D and CARTO), 4 maps per study and 8 studies, for a total of 96 possible simulated ablation points.

*Data transfer and processing.* All points used in the study comparison were acquired by Navik 3D. When a point was acquired by Navik 3D (via Take Point and added to a map's point list), all data relevant to Navik 3D's 2D-3D algorithm were logged to disk as a series of files, uniquely identified by the time/date the point was acquired. These data included: (a) fluoroscope gantry positions and angles, (b) fluoroscopic image frames (raw pixel data), and (c) approximate location of the distal electrode of the mapping catheter.

The data of interest consisted of 240 possible pairs of frame-grabbed sequences of Tagged Image File Format (TIFF) files collected by Navik 3D during the 8 experiments. It is not possible to see the tiny pacing electrodes that were critical to analyzing study results in the TIFF images.

The pacing electrodes are significantly smaller in physical dimension than the distal electrode of the mapping catheter; therefore, at the end of the study, the animal surgeon identified the pacing electrodes using a magnified version of the fluoroscopy images along with the diagram identifying the location of the electrodes. The images were then significantly further magnified offline by the evaluating statistician to identify the locations of interest in the pacing electrodes. ImageJ, the image-processing program developed by the NIH (16), was used to view, identify, and record the distal, centroid, and proximal ends of the active pacing electrode and was confirmed manually by a human over-reader.

Each pair of fluoroscopy sequences and gantry parameters contained the 2D information required for generating 3D location estimates of points of interest via a geometric ray tracing process known as back projection.

To quantify the proximity of the distal electrode of the mapping catheter to the pacing electrode for each simulated ablation point, back-projection fiducial points were identified along both the distal electrode of the mapping catheter and the active pacing electrode across the sequences in each view. Ideally, to quantify proximity to the pacing electrode, the fiducial needed to represent the points of closest approach of the ablation tip and the pacing electrode. Furthermore, the selection process needed to be as objective as possible. For these reasons, potential fiducial points were identified as follows: (a) along the distal electrode of the mapping catheter, the distal and centroid points were identified by an automated algorithm; and (b) along the active pacing electrode, the distal, centroid, and proximal points were identified manually using ImageJ.

From this set of 6 potential pairs of fiducial points, the pair that represented the closest approach of the ablation catheter's distal electrode and the pacing electrode (minimal distance) across the sequences being traced in both views was chosen as input for the back-projection algorithm as a primary analysis.

The  $1,000 \times 1,000$ -pixel fluoroscopic image sequences associated with each simulated ablation were embedded in larger frame-grabbed TIFF images generated by Navik 3D. ImageJ was used to view the frame-grabbed data. ImageJ also was used to magnify the region of interest of the fluoroscopy component of the frame-grabbed sequences and to mark and record the 2D distal, centroid, and proximal ends of the active pacing electrode.

The active pacing electrode was indicated in the details logged in the Experimental Procedure Records.

## Applying back projection to animal study data

*Ground truth description.* For the simulated ablation arm of this study, the ground truth with which both Navik 3D and CARTO were compared was the true 3D location of the catheter tip and pacing electrodes, as estimated via back projection. As explained earlier, the back-projection 3D reconstruction process uses 2 oblique fluoroscopy views of a fixed object within a defined 3D space. For each view, 3D projection lines

from source to object to detector were determined from the position of the object's shadow on the fluoroscopic image and the physical gantry parameters. The intersection of the 3D lines provided the 3D estimate of the object's position (17).

Back projection was used in stand-alone fashion during analysis of the simulated ablation study data to generate ground truth locations of the mapping/distal electrode of the mapping catheter and the pacing electrodes. The measures of interest in the animal study were the actual 3D distances of the distal electrode of the mapping catheter to the active pacing electrode for each simulated ablation for both Navik 3D and CARTO as compared with the back-projected 3D location of these electrodes.

*Analysis and selection of fiducial points for back projection.* For input into back projection, as described previously, 2 potential fiducial points were identified on the ablation tip and 3 potential fiducial points on the active pacing electrode across consecutive frames in oblique view pairs of fluoroscopy sequences acquired at identified simulated ablation points. For each oblique view pair of sequences, a single fiducial location was selected along the ablation tip and 1 along the pacing electrode. The selection process identified the pair of fiducial points that had minimal 3D separation, averaged over all tracked frames in each sequence and across all possible pair choices.

*Data analysis.* Data were collected on case report forms. Relevant data needed for processing and analysis were entered onto 2 spreadsheets, 1 for further processing for ground truth and statistical analysis and 1 for exposure times. The location information was processed, and a processing output spreadsheet was provided to the statistician for analysis. The statistical analysis was conducted using SAS software.

### Analysis of outliers

Of the 93 simulated ablation points evaluated for each device, 4 points were identified as outliers: 3 (3.22%) for CARTO in experiment 3, and 1 (1.07%) for Navik 3D in experiment 10. In these cases, it was determined that the mapping catheter had moved between acquisitions of the AP to LAO views.

Figure 10 depicts the 3 outlier simulated ablations in CARTO LV Map 2 in experiment 3. As shown in the figure, the catheter could not be brought to the same location during the 3 points. This could have been because of some motion or difficulty in approaching the earliest breakthrough point identified by CARTO. It is also possible that the true location was not correctly identified in this case. In either scenario, the number of outliers over the entire study was extremely small for both CARTO and Navik 3D.

### Conclusion

In conclusion, Navik 3D is a potentially unique system that recognizes that the 2D projection of the single-plane fluoroscopy system contains information about the position of the object in 3D. X-rays travel from a small, quasi-point x-ray source in a cone beam toward the patient, where they interact with the tissues of the patient and any objects within. Using these principles, the system developed by APN Health uses existing data from fluoroscopy and patient monitoring and recording systems to create 3D maps that will enable all EP labs to use 3D mapping for mapping and ablation procedures without infrastructure modification. As demonstrated by the phantom and animal study, Navik 3D is capable of performing in a beating heart with performance equivalent to the CARTO system. The techniques described here could potentially also be used in non-EP procedures.

### Statistics

In the study, Navik 3D minus CARTO distances (DN-DC) were formed. The proportion of DN-DC less than or equal to 2 mm being less than or equal to 0.75 was rejected via a 1-sided 95% bootstrap CI, concluding that Navik 3D was equivalent to CARTO. A Bland-Altman analysis revealed a negative mean difference, indicating a generally smaller Navik 3D distance. A regression (DN vs. DC) yielded a significant positive relationship ( $P < 0.0001$ ), and because points generally fell below a 45-degree line, Navik 3D distances were smaller. Since a 2-sided 95% intercept CI did not contain 1 ( $P = 0.01$ ), Navik 3D and CARTO performance was not the same. These analyses using the SAS system showed that Navik 3D performed in a beating heart.

### Study approval

All animal procedures were approved by and conducted in accordance with the IACUC at the Aurora Health Care Animal Research Facility. Aurora Health Care's Animal Welfare Assurance (A3704-01) is on file with the Office of Laboratory Animal Welfare. Human subjects were not involved.



## Author contributions

JS conceived, designed, and served as investigator on the research study and wrote the manuscript. DK conducted the phantom experiment, and DK and IC conducted the animal experiment. DK acquired the data in both experiments. DK, BB, MP, DB, and DR analyzed data and contributed to the manuscript.

## Acknowledgments

This work was funded in part by APN Health, LLC. The authors are grateful to Jennifer Pfaff and Susan Nord of Aurora Cardiovascular Services for editorial preparation of the manuscript and Brian Miller and Brian Schurrer of Aurora Research Institute for help with the figures.

Address correspondence to: Jasbir Sra, Aurora Cardiovascular Services, Aurora St. Luke's Medical Center, 2801 W. Kinnickinnic River Parkway, Suite 840, Milwaukee, Wisconsin 53215, USA. Phone: 414.649.3909; E-mail: publishing1@aurora.org.

1. Blomström-Lundqvist C, et al. ACC/AHA/ESC guidelines for the management of patients with supraventricular arrhythmias—executive summary: a report of the American College of Cardiology/American Heart Association Task Force on Practice Guidelines and the European Society of Cardiology Committee for Practice Guidelines (Writing Committee to Develop Guidelines for the Management of Patients With Supraventricular Arrhythmias). *Circulation*. 2003;108(15):1871–1909.
2. Aliot EM, et al. EHRA/HRS Expert Consensus on Catheter Ablation of Ventricular Arrhythmias: developed in a partnership with the European Heart Rhythm Association (EHRA), a Registered Branch of the European Society of Cardiology (ESC), and the Heart Rhythm Society (HRS); in collaboration with the American College of Cardiology (ACC) and the American Heart Association (AHA). *Heart Rhythm*. 2009;6(6):886–933.
3. Calkins H, et al. 2012 HRS/EHRA/ECAS expert consensus statement on catheter and surgical ablation of atrial fibrillation: recommendations for patient selection, procedural techniques, patient management and follow-up, definitions, endpoints, and research trial design: a report of the Heart Rhythm Society (HRS) Task Force on Catheter and Surgical Ablation of Atrial Fibrillation. Developed in partnership with the European Heart Rhythm Association (EHRA), a registered branch of the European Society of Cardiology (ESC) and the European Cardiac Arrhythmia Society (ECAS); and in collaboration with the American College of Cardiology (ACC), American Heart Association (AHA), the Asia Pacific Heart Rhythm Society (APHRS), and the Society of Thoracic Surgeons (STS). Endorsed by the governing bodies of the American College of Cardiology Foundation, the American Heart Association, the European Cardiac Arrhythmia Society, the European Heart Rhythm Association, the Society of Thoracic Surgeons, the Asia Pacific Heart Rhythm Society, and the Heart Rhythm Society. *Heart Rhythm*. 2012;9(4):632–696.e21.
4. Goren A, Liu X, Gupta S, Simon TA, Phatak H. Quality of life, activity impairment, and healthcare resource utilization associated with atrial fibrillation in the US National Health and Wellness Survey. *PLoS One*. 2013;8(8):e71264.
5. Ben-Haim SA, Osadchy D, Schuster I, Gepstein L, Hayam G, Josephson ME. Nonfluoroscopic, in vivo navigation and mapping technology. *Nat Med*. 1996;2(12):1393–1395.
6. Sra J, Akhtar M. Mapping techniques for atrial fibrillation ablation. *Curr Probl Cardiol*. 2007;32(12):669–767.
7. Packer DL. Three-dimensional mapping in interventional electrophysiology: assets and limitations of 3D mapping systems. *J Cardiovasc Electrophysiol*. 2005;16(10):1110–1116.
8. US Market for Electrophysiology Mapping Ablation Devices to Reach Value of over \$1.6 Billion by 2016 [press release]. Toronto: Business Wire; June 12, 2012.
9. Efron B, ed. *The Jackknife, the Bootstrap and Other Resampling Plans*. Philadelphia, PA: Society for Industrial and Applied Mathematics; 1982.
10. Bland JM, Altman DG. Agreement between methods of measurement with multiple observations per individual. *J Biopharm Stat*. 2007;17(4):571–582.
11. Lickfett L, et al. Radiation exposure during catheter ablation of atrial fibrillation. *Circulation*. 2004;110(19):3003–3010.
12. Hirsh J, Anand SS, Halperin JL, Fuster V, American Heart Association. Guide to anticoagulant therapy: Heparin : a statement for healthcare professionals from the American Heart Association. *Circulation*. 2001;103(24):2994–3018.
13. Liang KY, Zeger SL. Longitudinal data analysis using generalized linear models. *Biometrika*. 1986;73(1):13–22.
14. Nakagawa H, et al. Inverse relationship between electrode size and lesion size during radiofrequency ablation with active electrode cooling. *Circulation*. 1998;98(5):458–465.
15. Lin JL, Wilber DJ, Du D, Pearlman J, Ruskin JN, Garan H. Localization of breakthrough site of canine monomorphic ventricular tachycardia by pacemapping. A vectorial approach. *Circulation*. 1991;84(3):1319–1332.
16. Schneider CA, Rasband WS, Eliceiri KW. NIH Image to ImageJ: 25 years of image analysis. *Nat Methods*. 2012;9(7):671–675.
17. Rougée A, Picard CL, Troussset YL, Ponchut C. Geometrical calibration for 3D x-ray imaging. *Proc SPIE*. 1993;1897:161–168.